Metamagnetism and weak ferromagnetism in nickel (II) oxalate crystals



2012 J. Phys.: Condens. Matter 24 196003

(http://iopscience.iop.org/0953-8984/24/19/196003)

J. Phys.: Condens. Matter **24** (2012) 196003 (5pp) doi:10.1088/0953-8984/24/19/196003

# Metamagnetism and weak ferromagnetism in nickel (II) oxalate crystals

**E Romero-Tela[1], M E Mendoza[1] and R Escudero[2]**

[1] Instituto de Física, Benemérita Universidad Autónoma de Puebla, Apartado Postal J-48, Puebla 72570, Mexico
[2] Instituto de Investigaciones en Materiales, Universidad Nacional Autónoma de México, Apartado Postal 70-360, México DF 04510, Mexico

E-mail: evarotel@gmail.com

Received 11 November 2011, in final form 1 March 2012
Published 19 April 2012
Online at stacks.iop.org/JPhysCM/24/196003

**Abstract**
Microcrystals of orthorhombic nickel (II) oxalate dihydrate were synthesized through a precipitation reaction of aqueous solutions of nickel chloride and oxalic acid. Magnetic susceptibility exhibits a sharp peak at 3.3 K and a broad rounded maximum near 43 K. We associated the lower maximum with a metamagnetic transition that occurs when the magnetic field is about ≥3.5 T. The maximum at 43 K is typical of 1D antiferromagnets, whereas weak ferromagnetism behavior was observed in the range of 3.3–43 K.

(Some figures may appear in colour only in the online journal)

## 1. Introduction

It has been shown, theoretically and experimentally, that if a critical magnetic field $H$ is applied along the crystalline anisotropy axis of an antiferromagnet (AF), there occurs a nearly 90° rotation of the sublattice vectors. An antiferromagnetic material with such a behavior is known as a metamagnet [1, 2]. This behavior has been observed in compounds like: $CuCl_2{\cdot}2H_2O$ [3], $FePt_3$, YCO, $TiBe_2$ [4] and $Ni(C_2O_4)$(bpy), where bpy = 4, 4′-bipyridine($C_{10}H_8N_2$) [5], when applying high magnetic fields (from 10 to 50 T). The type of ordering in $Fe(C_2O_4)$(bpy) and $Co(C_2O_4)$(bpy) is also antiferromagnetic but with canted spins. This uncompensated antiferromagnetism produces weak ferromagnetism (WF). Recently, investigations in the quasi-one-dimensional magnetic compound $\beta$-$CoC_2O_4{\cdot}2H_2O$ [6] revealed that the intra- and interchain magnetic interactions tilt the spins, distorting the antiferromagnetic order and producing the WF.

The orthorhombic $\beta$ phase of nickel oxalate dihydrate belongs to the space group *Cccm* with cell parameters $a = 11.842(2)$ Å, $b = 5.345(1)$ Å and $c = 15.716(2)$ Å [7]. In this structure, oxalate bridges link $Ni^{2+}$ ion chains along the $b$ direction [8–11] and they mediate a dominant antiferromagnetic intrachain superexchange interaction [12]. Its molar susceptibility data exhibits the broad rounded maximum typical of 1D antiferromagnets with $T_{max} \sim 41$ K [13].

In this paper we report results on the synthesis, crystal structure and magnetic measurements of the orthorhombic $\beta$-$NiC_2O_4{\cdot}2H_2O$ microcrystals. We determined by isothermal $M$–$H$ measurements, from 2 to 80 K, that this phase exhibits weak ferromagnetism in the range of 3.3–43 K. At low temperature a metamagnetic order is observed under an applied field ≥3.5 T, in $\chi$–$T$ measurements.

## 2. Experimental methods

The synthesis of $\beta$-nickel oxalate dihydrate under nitrogen atmosphere was carried out by the precipitation reaction of aqueous solutions of nickel (II) chloride 0.1 M (Aesar, 99.9995%) and oxalic acid 0.00625 M (Baker, ≥99.9%), following the chemical equation

$$H_2C_2O_{4(aq)} + NiCl_{2(aq)} \rightarrow NiC_2O_4{\cdot}2H_2O_{(s)} + 2HCl_{(aq)}.$$

The precipitates were filtered and dried at room temperature. Morphological analyses were performed with

 

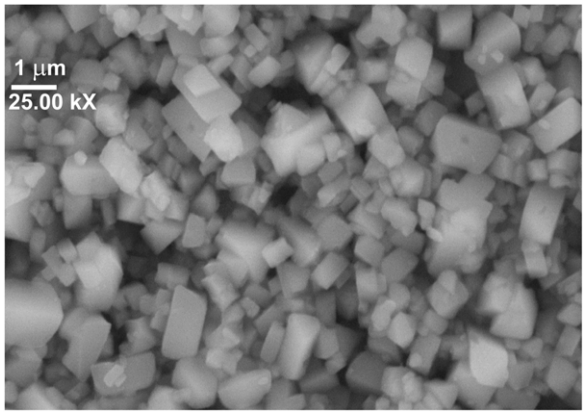


**Figure 1.** SEM micrographs of $\beta$-nickel oxalate dihydrate shows prismatic-like shapes. Average length size ($L$) and diameter ($D$) were 1.47 and 0.65 $\mu$m, respectively.

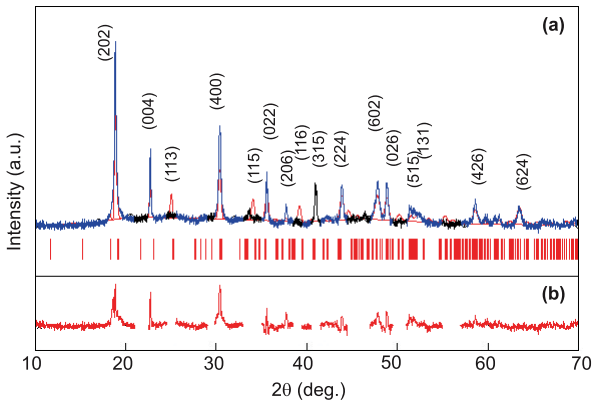


**Figure 2.** (a) X-ray powder diffraction pattern of nickel oxalate dihydrate (blue), peaks absent (black), Rietveld calculated pattern (red) and Miller index (red lines) reported for the orthorhombic *Cccm* phase (JCPDS file: 25-0250). (b) Difference pattern (red).

a scanning electron microscope (SEM, Cambridge-Leica Stereoscan 440). Powder x-ray diffraction patterns were acquired using a Siemens D5000 diffractometer operating in the Bragg–Brentano geometry with $\lambda$ (Cu K$\alpha$) = 1.541 Å and $2\theta$ scan from 10° to 70°and step size of 0.02°. Thermogravimetric (TG) and differential thermal analysis (DTA) curves were obtained in a SDT-TA Instruments model 2960 in air atmosphere with a heating rate of 5 °C min$^{-1}$, from room temperature up to 600 °C. Magnetization measurements were done with a Quantum Design MPMS SQUID magnetometer, MPMS-5. Zero-field-cooling (ZFC) and field-cooling (FC) cycles were performed at magnetic field intensities from 0.01 to 5.00 T in the range 2 up to 250 K. Isothermal magnetization measurements $M(H)$ were obtained from 2 to 80 K. The diamagnetic contribution calculated from Pascal's constants [14] was $\chi_{Di} = -72 \times 10^{-6}$ cm$^3$ mol$^{-1}$.

## 3. Results and discussion

### *3.1. Synthesis*

Prismatic green microcrystals of nickel oxalate dihydrate were obtained after eight days of growth in nitrogen atmosphere. Figure 1 presents a SEM micrograph of the crystals with an average length size ($L$) and diameter ($D$) of 1.47 and 0.65 $\mu$m, respectively. Chemical analysis by digestion/ICP-OEP, combustion/TCD/IR-detection and pyrolysis/IR-detection gave the composition in weight of 31.82% in nickel, 13.21% in carbon, 2.48% in hydrogen and 51.00% in oxygen.

### *3.2. Structural characterization*

Figure 2(a) displays the XRD powder diffraction pattern of $NiC_2O_4{\cdot}2H_2O$ (blue pattern); it is in good agreement with the reported (red lines) for the orthorhombic $\beta$ phase of cobalt oxalate dihydrate (JCPDS file: 25-0250). This figure also shows the Rietveld profile fit (red pattern). In figure 2(b) the difference pattern (red) obtained by using the Win-Rietveld software [15]. Background was

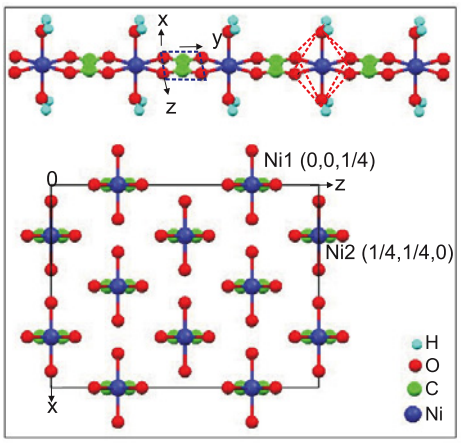


**Figure 3.** Ni oxalate unit cell of the orthorhombic $\beta$ phase of space group *Cccm* (JCPDS file: 25-0250). The eight nickel atoms are located in two non-equivalent positions designated as Ni1 and Ni2.

estimated by linear interpolation and the peak shape was modeled by a pseudo-Voigt function. Unit cell parameters were $a$ = 11.842 Å, $b$ = 5.345 Å and $c$ = 15.716 Å [7]. The atomic positions were those reported by Deyrieux *et al* for iron oxalate [10], i.e. 4Co($\frac{1}{4}$, $\frac{1}{4}$, 0), 4Co(0, 0, $\frac{1}{4}$), 8C$_{oxalate}$($\frac{1}{4}$, $\frac{1}{4}$, 0.042), 8C$_{oxalate}$(0, $\frac{1}{2}$, 0.042), 16O$_{oxalate}$($\frac{1}{4}$, 0.0941, 0.089), 16O$_{oxalate}$(0, 0.691, 0.339), 8O$_{water}$(0.423, $\frac{1}{4}$, 0) and 8O$_{water}$(0.173, 0, $\frac{1}{4}$). The weighted profile and expected residual factors obtained in the refinement were $R_{wp}$ = 32.52 and $R_{exp}$ = 13.52.

It must be noticed that some low intensity calculated peaks were absent in the experimental pattern (black peaks in figure 2(a)); this could be due to the method of preparation.

Refined cell parameters determined for the orthorhombic phase of the Ni oxalate sample were $a$ = 11.759(3) Å, $b$ = 5.327(1) Å and $c$ = 15.654(4) Å. Schematic representation of the unit cell is shown in figure 3. There are two non-equivalent positions for nickel ions, designated as Ni1 and Ni2: each nickel ion is shifted in respect to the other by a translation vector ($\frac{1}{2}$, $\frac{1}{2}$, 0).

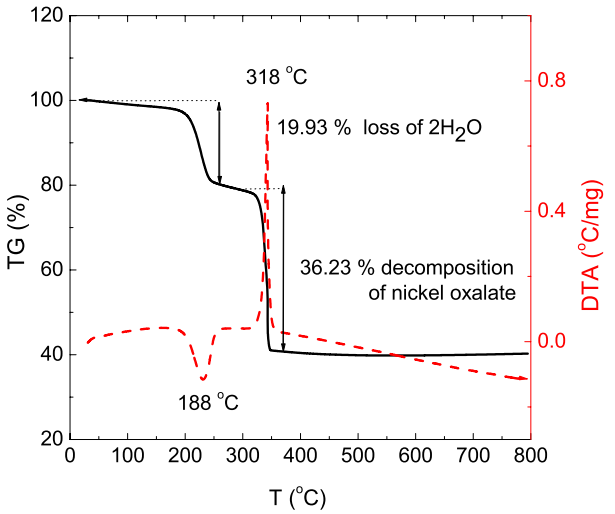


**Figure 4.** The TG (solid)/DTA (dashed) curves for $NiC_2O_4{\cdot}2H_2O$ at 5 °C $min^{-1}$ heating rate.

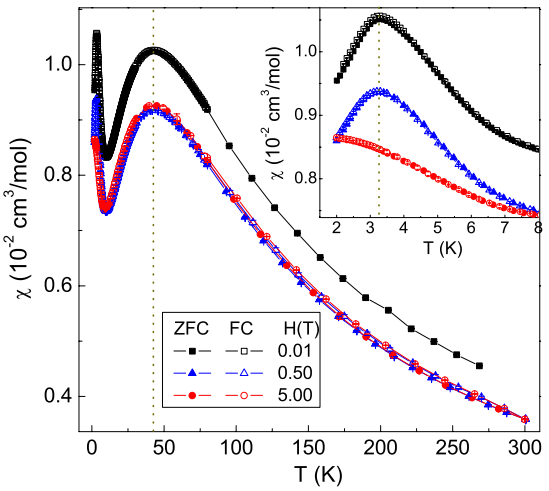


**Figure 5.** Main panel: molar susceptibility of $\beta$-$NiC_2O_4{\cdot}2H_2O$ with maximum at around 43 K, for both ZFC and FC modes, measured with three applied fields: 0.01, 0.50 and 5.00 T. Inset displays the susceptibility at low temperature. The maximum at about 3.3 K changes and disappears when the applied magnetic field exceeds 5 T.

Finally, the coherent diffraction size ($D$) for the sample crystallites was calculated with the Scherrer equation [16] using the (202) peak; the calculated value was 21.4 nm.

### *3.3. Thermal analysis*

Figure 4 shows the TG and DTA curves of $NiC_2O_4{\cdot}2H_2O$. Two steps of weight loss were observed, the first one ending at 188 °C and the second one finishing at 318 °C. In the first step the weight loss of 19.93% corresponds to the loss of two water molecules, which agrees with the theoretical value of 19.73%. The DTA curve associated with this process shows an endothermic peak at 188 °C. The dehydration reaction is

$$NiC_2O_4{\cdot}2H_2O_{(s)} \rightarrow NiC_2O_{4(s)} + 2H_2O. \qquad (1)$$

The weight loss of about 36.23% in the second step may be associated with the decomposition of the anhydrous nickel oxalate to nickel oxide; this agrees with the theoretical value of 39.85% [17, 18]. The corresponding DTA curve shows an exothermic peak at $T = 318$ °C. The decomposition reaction in this step can be written as

$$NiC_2O_{4(s)} \rightarrow NiO_{(s)} + CO_{2(g)} + CO_{(g)}. \qquad (2)$$

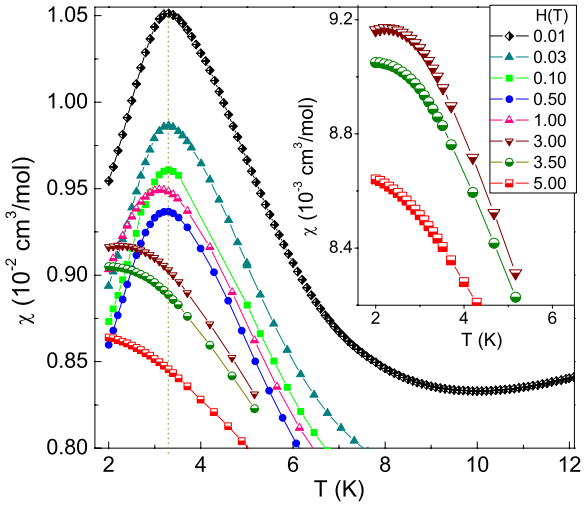


**Figure 6.** This figure presents in the main panel the molar susceptibility at low temperature with applied fields from 0.01 to 5.00 T. Clearly seen is the evolution of the molar susceptibility with increasing field. The inset displays three curves measured with magnetic fields from 3 to 5 T. At a field about 3.5 T the maximum at 3.3 K disappears.

### *3.4. Magnetic measurements*

The molar susceptibility $\chi(T)$ for the sample is shown in figure 5. It was measured by applying magnetic fields of 0.01, 0.50 and 5.00 T in both ZFC, and FC modes. The main panel shows two well-defined maxima in the susceptibility at 3.3 and 43 K. We also observed changes in the susceptibility at 3.3 K when the magnetic field exceeds 5 T, as mentioned in the caption of figure 5.

Figure 6 shows susceptibility measurements $\chi(T)$ at magnetic fields from 0.01 to 5 T. Those results indicated that, at a field of 3.5 T, the peak at $T = 3.3$ K disappears. This change in the magnetic behavior is related to a metamagnetic transition. Thus, the applied field $\geq$3.5 T, in this compound, is the critical field at which the constraints of crystal field are exceeded and the magnetic behavior changes.

These results can be compared with those found in other $Ni^{2+}$ systems. Evidence of a metamagnetic transition in $Ni(C_2O_4)(bpy)$ was also obtained in polycrystalline materials [5]. The transition has been anticipated by slope changes in $M(H)$ with higher applied fields, i.e. $H >$ 30 kG and below $T_N = 26$ K. In this compound, the one-dimensional magnetic character can be enhanced by replacing the transaxial aquo group by organic groups, such

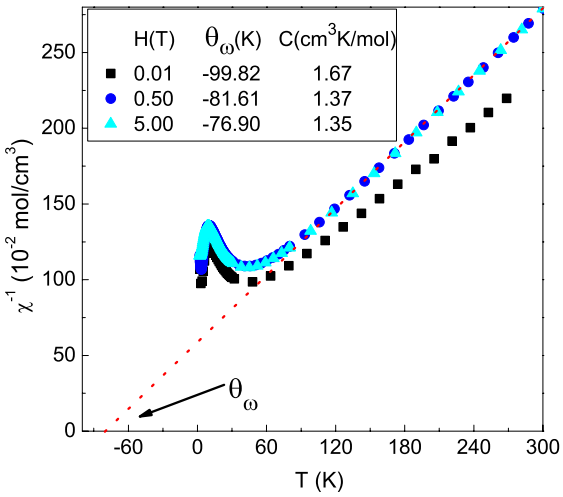


**Figure 7.** Inverse susceptibility at different magnetic fields, $\chi^{-1}(T)$, for dihydrate nickel oxalate. The Weiss temperature, $\theta_\omega$, changes from about −76.90 to −99.82 K. The Curie constant also changes from 1.35 to 1.67 cm$^3$ mol$^{-1}$ K, from high to low magnetic fields.

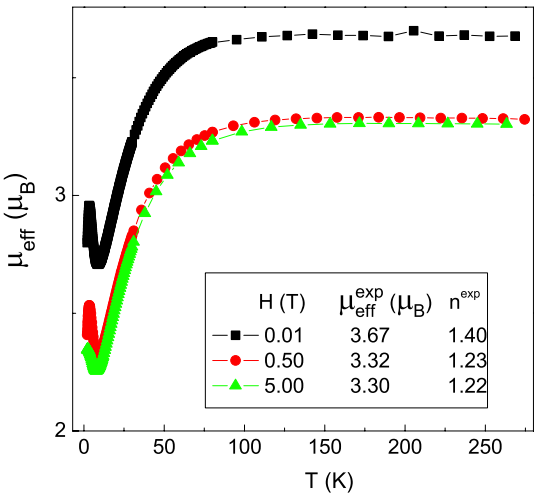


**Figure 8.** Effective Bohr magneton moments $\mu_{\rm eff}$ per mol as a function of temperature. At room temperature the values change from 3.30 to about 3.67 $\mu_{\rm B}$, depending on the magnetic field applied. $n^{\rm exp}$ is the number of unpaired electrons.

as bipyridine. This has the effect of reducing the interchain interaction and consequently the Néel temperature, and the critical fields required for the metamagnetic transitions [19, 20]. Important examples of this behavior are $CoCl_2{\cdot}2H_2O$ and $\alpha$-Co(pyridine)$_2$Cl$_2$ [21]. The details of the magnetic properties of these materials are best understood by examining single-crystal data because the transitions are sensitive to the orientation of the applied field [1].

It is important to mention that, in figure 5, we show that the magnetic susceptibility presents a wide maximum at about 43 K. From 100 K to room temperature $\chi(T)$ smoothly decreases and a paramagnetic Curie–Weiss behavior can be fitted. The maximum value at 43 K changes with the magnetic field applied as shown in this figure. The changes are in the range from $0.91 \times 10^{-2}$ to $1.03 \times 10^{-2}$ cm$^3$ mol$^{-1}$. This behavior is quite similar to that reported in other compounds, such as Ni(pip)($C_2O_4$), where pip = piperazine, which is formed by chains of $[Ni(ox)]_n$ and $[Ni(pip)]_n$. In that example, a broad maximum is observed and occurs at 53(1) K [22]. So, accordingly the broad maximum in the susceptibility in our compound is typical behavior of a low-dimensional antiferromagnetic system [23].

In figure 7 we show a plot of the inverse of susceptibility, $\chi(T)^{-1}$ at $H = 0.01$, 0.50 and 5.00 T, for $\beta$-$Ni_2O_4{\cdot}2H_2O$. The analysis of these measurements was performed by fitting a Curie–Weiss curve from room temperature to 100 K. The fitting parameters were Weiss temperature $\theta_\omega$ and Curie constant $C$ varying from −76.90 to −99.82 K and from 1.35 to 1.67 cm$^3$ mol$^{-1}$ K, respectively.

The fitting parameters could be used to calculate the effective magnetic moment $\mu_{\rm eff}$ per mole from the equation $\mu_{\rm eff} = 2.84[C]^{1/2} = 2.84[\chi T]^{1/2}$, which is shown in figure 8.

An important aspect of the behavior, $\mu_{\rm eff}$, for this compound, and related to the Curie constant and the large negative Weiss constant, is indicative of a significant antiferromagnetic exchange interaction between neighboring nickel ions, and a large degree of frustration [24]. It is quite possible because of the metamagnetic transition obtained in figures 5 and 6. As observed, this dramatic change in the $\mu_{\rm eff}$ is the effect of the change of the Curie constant, and then via the number of unpaired electrons. Thus, according to $\mu_{\rm eff} = g[n(n+1)]^{1/2}$, the number of unpaired electrons $n$ in $NiC_2O_4{\cdot}2H_2O$ can be calculated as 1.40, 1.23 and 1.22, respectively, for applied fields of 0.01 T, 0.50 T and 5.0 T.

In order to understand more about the magnetic characteristics of this oxalate, we studied the *M–H* isothermal measurements from the temperature range 2–80 K (see figure 9). From these data we extracted the coercive field, which shows a small measurable and perceptible exchange bias. Our measurements of the coercive field, although small, were carefully checked and are below the possible errors. The results are displayed in figure 10.

This exchange bias can be explained as the effect of inter- and intrachain interactions in this compound. The interaction of metallic ions between chains is at the origin of spin canting. This small but measurable exchange bias indicates that, instead of producing a pure antiferromagnetic order, the magnetic order has been distorted by canted spins, giving rise to weak ferromagnetism. Since weak ferromagnets are a delicate balance of opposing forces, it is not surprising to find that many are also metamagnets [25].

Experimentally, it is important to mention that great care was taken when measuring the exchange bias. Our SQUID magnetometer is provided with a mu-metal shielding. At the moment of performing the magnetization measurements a flux gate magnetometer was used to demagnetize the superconducting coil. This procedure reduces the magnetic field to a very small value of about 0.001 G or less and the mu shielding eliminates external magnetic influences, such as the Earth's magnetic field.

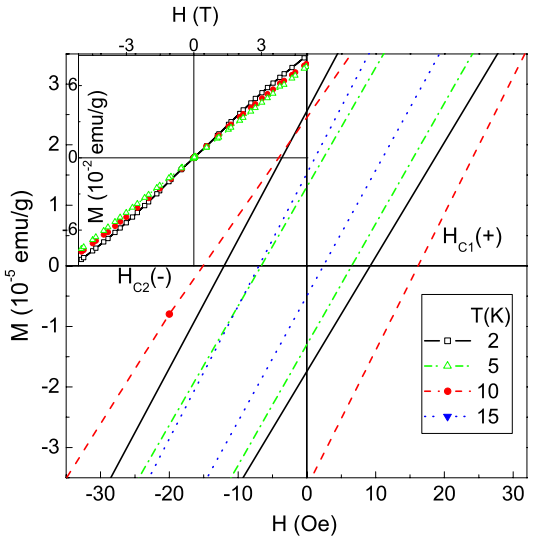


**Figure 9.** Isothermal magnetization measurements $M$–$H$ from 2 to 15 K shown in the main panel. Note the coercive field and the small exchange bias. Inset shows the $M(H)$ measurements at 4 T and different temperatures from 2 to 80 K. At low fields (main panel) the hysteretic effect is clearly observed. The asymmetric behavior in the coercive field is related to a exchange bias effect due to canted spins, but another type of interaction is not discarded as driven by Dzyaloshinsky–Moriya type exchange (DM).

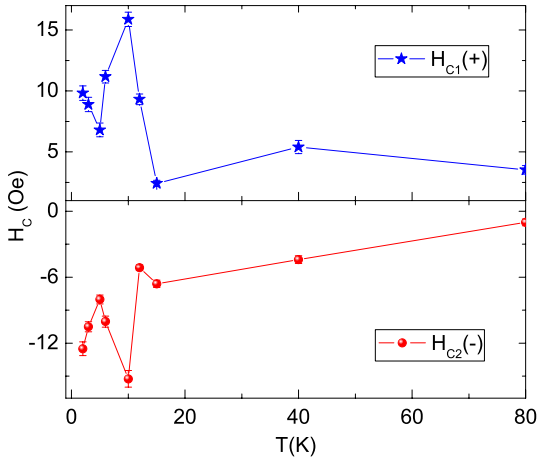


**Figure 10.** Coercive field versus temperature determined by isothermal magnetic measurements.

## 4. Conclusions

Single-phase microcrystals of orthorhombic nickel (II) oxalate dihydrate were prepared by soft solution chemistry, as observed by XRD powder diffraction. Chemical analysis, DTA and TG studies revealed that the microcrystals are of high purity. $\chi(T)$ measurements showed the existence of two maxima at 3.3 and at 43 K. The first one at low temperature changes and disappears with applied magnetic field. This change is due to a metamagnetic transition: the maximum disappears with an applied field of about $\geq$3.5 T. The second maximum indicates an antiferromagnetic order, with interactions due to coupled chains via inter- and intrachain interactions and/or DM-type exchange. The effects of interchain interactions disturb the AF coupling, distorting it and canting spins, which in turn produce a weak ferromagnetic order. This WF is evident by hysteresis measurements in $M$–$H$ isothermal measurements.

## Acknowledgments

Partial support for this work is gratefully acknowledged from CONACyT, project no. 44296/A-1 and Scholarship CONACyT, register no. 188436 for ER-T; VIEP-BUAP, project no. MEAM-EXC10-G. RE, thanks to CONACyT Project 129293 (Ciencia Básica), DGAPA-UNAM project no. IN100711, project BISNANO 2011 and project PICCO 11-7 by the Department of Distrito Federal, México.

## References

[1] Keffer F and Chow H 1973 *Phys. Rev. Lett.* **31** 1061
[2] Jones E R Jr and Stone J A 1972 *J. Chem. Phys.* **56** 1343
[3] Liu T, Zhang Y, Wang Z and Gao S 2006 *Inorg. Chem.* **45** 2782
[4] Hurd C M 1982 *Contemp. Phys.* **23** 469
[5] Yuen T, Lin C L and Mihalisin T W 2000 *J. Appl. Phys.* **87** 6001
[6] Romero E, Mendoza M E and Escudero R 2011 *Phys. Status Solidi* b **248** 1519
[7] Deyrieux R, Berro C and Péneloux A 1973 *Bull. Soc. Chim. Fr.* **1** 25
[8] Dubernat P J and Pezerat H 1974 *J. Appl. Crystallogr.* **7** 378
[9] Molinier M, Price D J, Wood P T and Powell A K 1997 *J. Chem. Soc. Dalton Trans.* 4061
[10] Deyrieux R and Péneloux A 1969 *Bull. Soc. Chim. Fr.* 2675
[11] Drouet C, Pierre A and Rousset A 1999 *Solid State Ion.* **123** 25
[12] Kurmoo M 2009 *Chem. Soc. Rev.* **38** 1353
[13] Vaidya S, Rastogi P, Agarwal S, Gupta S K, Ahmad T, Antonelli A M, Ramanujachary K V, Lofland S E and Ganguli K 2008 *J. Phys. Chem.* C **112** 12610
[14] Bain G A and Berry J F 2008 *J. Chem. Educ.* **85** 532
[15] McCusker L B, Von Dreele R B, Cox D E, Louër D and Scardi P 1999 *J. Appl. Crystallogr.* **32** 36
[16] Cullity B D 1978 *Elements of X-ray Diffraction* 2nd edn (Reading, MA: Addison-Wesley)
[17] Zhan D, Cong C, Diakite K, Tao Y and Zhang K 2005 *Thermochim. Acta* **430** 101
[18] Zakharov A N, Mayorova A F and Perov N S 2008 *J. Therm. Anal. Calorim.* **92** 747
[19] Otieno T and Thompson R C 1995 *Can. J. Chem.* **73** 275
[20] Mao L, Rettig S J, Thompson R C, Trotter J and Xia S 1996 *Can. J. Chem.* **74** 433
[21] Foner S, Frankel R B, Reiff W M, Wong H and Long G J 1978 *J. Chem. Phys.* **68** 4781
[22] Keene T-D, Ogilvie H R, Hursthouse M B and Price D J 2004 *Eur. J. Inorg. Chem.* **2004** 1007
[23] Bonner J C and Fisher M E 1964 *Phys. Rev.* A **135** 640
[24] Ramirez A P 2001 *Handbook of Magnetic Materials* 13 edn, ed K H J Huschow (Amsterdam: North-Holland) p 423
[25] Stryjewski E and Giordano N 1977 *Adv. Phys.* **26** 487